General Disclaimer

One or more of the Following Statements may affect this Document

- This document has been reproduced from the best copy furnished by the organizational source. It is being released in the interest of making available as much information as possible.

- This document may contain data, which exceeds the sheet parameters. It was furnished in this condition by the organizational source and is the best copy available.

- This document may contain tone-on-tone or color graphs, charts and/or pictures, which have been reproduced in black and white.

- This document is paginated as submitted by the original source.

- Portions of this document are not fully legible due to the historical nature of some of the material. However, it is the best reproduction available from the original submission.

NASA Technical Memorandum 83014

Parallel Plate Radiofrequency Ion Thruster

Shigeo Nakanishi
Lewis Research Center
Cleveland, Ohio

Prepared for the
Sixteenth International Electric Propulsion Conference
cosponsored by the American Institute of Aeronautics and Astronautics,
the Japan Society for Aeronautical and Space Sciences,
and Deutsche Gesselschaft fur Luft- und Raumfahrt
New Orleans, Louisiana, November 17–19, 1982

NASA

PARALLEL PLATE RADIOFREQUENCY ION THRUSTER

Shigeo Nakanishi

National Aeronautics and Space Administration
Lewis Research Center
Cleveland, Ohio 44135

Abstract

An 8-cm-diam. argon ion thruster is described which is operated by applying 100 to 160 MHz rf power across a thin plasma volume in a strongly divergent static magnetic field. No cathode or electron emitter is required to sustain a continuous wave plasma discharge over a broad range of propellant gas flow. Preliminary results indicate that a large fraction of the incident power is being reflected by impedance mismatching in the coupling structure. Resonance effects due to plasma thickness, magnetic field strength, and distribution are presented. Typical discharge losses obtained to date are 500 to 600 W per beam ampere at extracted beam currents up to 60 mA.

Introduction

Advent of the Space Shuttle and possible construction of large space systems in near Earth orbit make inert gas propellants such as argon attractive because of its availability, system integration considerations, and such performance issues as simplicity and rapid startup characteristics. In a power-limited space system, the energy required to produce thrust is a major issue for electric propulsion. Reducing the discharge loss or energy required to produce a beam ion, therefore, has been one of the principle objectives of electrostatic ion thruster technology.

Recently, great strides have been made in the technology of large dc discharge ion thrusters using argon.[1, 2, 3] In fact, by using magnetic cusp geometries, the discharge performance with inert gas propellants has surpassed what was once considered achievable only with mercury.

The high frequency gaseous discharge is an alternative means of producing the plasma from which beam ions are extracted. Electrodeless discharges using rf or microwave power have been discussed in the literature. The first adaptation to an ion thruster is probably the Giessen engine[4] and subsequent development of the RIT system[5]. More recently, some effort in the United States has been devoted to the high frequency generation of plasmas for ion thruster application.[6, 7, 8] The high frequency method provides the possibility of a great variety of ways by which electromagnetic energy can be coupled to a discharge plasma. It further permits use of promising geometrical configurations and propellants such as oxygen not usable in a dc discharge.

A program has been under way for preliminary investigations and evaluations of the discharge chamber performance, potentials, and limitations of novel rf ion thruster concepts. The parallel plate ion thruster, described herein, is one such concept of high frequency plasma generation. The configuration has been adapted to a set of conventional electrostatic ion extraction grids to produce an ion beam. Some effects of applied static magnetic field on source performance are evaluated because of the dominant effect that magnetic cusp fields have had on dc ion thrusters. The characteristics of rf power coupling to the plasma are examined and thruster performance in terms of absorbed power per ampere of extracted beam current is presented.

Apparatus and procedures

The absorbed power density in high frequency discharges may be expressed in the following form:

$$P = \frac{N_e e^2}{m_e \nu_e} \frac{\nu_e^2}{\nu_e^2 + \omega^2} \frac{E_o^2}{2} \qquad (1)$$

where

P absorbed power density, W/m^3

N_e electron density, m^{-3}

e electronic charge, coulomb

m_e electron mass, kg

ν_e effective electron-neutral collision frequency, sec^{-1}

ω input frequency, sec^{-1}

E_o spatial electric field, V/m

In electrostatic ion thrusters, a particular beam current density implies a certain plasma discharge number density upstream of the ion extraction grids. A given plasma density (represented by electron number density n_e in the equation) dictates the power per unit volume absorbed by the plasma for a given applied frequency, neutral density, and electric field. It follows that the total power required to sustain this plasma is a minimum when the plasma volume is a minimum. The parallel plate ion thruster configuration attempts to minimize the plasma volume by producing the plasma immediately upstream of the extraction grids in a thin cylindrical region of diameter, equal to that of the thruster ion extraction region. Losses in the plasma will also be reduced if the ions can be produced near or within the extraction sheath adjacent to the grids. This approach cannot be used in dc discharge thrusters because attempts to approach this situation by using short ion chambers have resulted in instability and/or inability to sustain the discharge.[9, 10]

A schematic cross section of the thruster is shown in Figure 1. It is one of two approaches suggested by Asmussen; the other approach (microwave plasma disk) is the subject of a companion paper.[11] A stainless steel cylindrical shell, 8 cm diam. by 7.4 cm long, constituted the thruster body. A flange on the downstream or forward end of the body maintained the required circular shape and also served as a mounting surface for the ion accelerator grids. The grids were conventional 8-cm thruster-dished optics but spaced with 0.51-mm-thick iso-mica around the periphery and clamped together to the body flange with paper clips.

Argon gas was introduced into the ionization chamber by a 3.18-mm-diam. tubular manifold with discharge holes drilled to direct the propellant rearward. A 1.5-mm-thick quartz cylinder lined the inside wall of the chamber to prevent arcing and breakdown discharge between the rf coupler plate and thruster body. The rf coupler plate was a 0.89-mm-thick copper disk mounted on one end of a length of RG 217-U coaxial cable which has a characteristic impedance of 50 ohms. The other end of the cable was fitted with a 50-ohm type N connector. The cable with exterior insulation removed was housed within a 1.27-cm diam. copper tubing to provide a rigid sliding member. The forward end of the copper tubing held a second copper disk to shield out rf from the rearward part of the chamber. Two 6.35-mm-thick boron nitride disks separated the rear copper disk and the front coupler plate. The thruster assembly was mounted at the rear on a round brass disk fitted inside the thruster body. The brass disk was mounted on a 1.27-cm-thick fiber plate whose circular periphery served as a conforming surface for the ground screen covering.

The two magnet coils were fabricated from 1.27-cm-wide by 0.13-mm-thick anodized aluminum ribbon wound on aluminum spools. The two end plates of the spools were removable and replaceable. This allowed the application of a thin adhesive film of polyimide insulation to prevent edge shorting of the aluminum ribbon. The larger and smaller of the magnet coils contained 600 and 220 turns, respectively.

The two magnet coils were mounted free of the thruster on the fiber plate to permit axial position adjustments.

The power system for the thruster was the same as that used previously for a slow wave antenna experiment.[8] A frequency variable oscillator was used to drive an rf power amplifier capable of delivering 500 W into a 50-ohms impedance at frequencies up to 160 MHz. An in-line rf power meter was used to measure incident and reflected powers. The entire power system was isolated from ground across a 115-V ac line transformer to permit high voltage ion-beam extraction.

The net acceleration potential applied to the screen, or upstream, grid was 1100 V and the accelerator grid was kept at -300 V. Although a tantalum wire neutralizer was used initially, at the beam voltage and current levels tested, facility ground neutralization was found adequate. Startup and operating procedures were very simple. A starting argon flow of about 2.8×10^{-7} kg/sec was established and about 80 W of rf power were applied. If the plasma discharge did not selfstart, a Tesla coil discharge across a spark gap downstream of the accelerator grids assured a start. An alternate and more convenient method of starting was to apply a sudden burst of voltage from the positive high voltage (screen) power supply. No breakdown across the ion optics was discernible but this approach always obtained ignition at test conditions of rf power and propellant flow so that subsequent readjustments were not necessary.

To set or change operating conditions, the grid to coupler plate gap was adjusted for maximum beam output. The magnet coil currents were then adjusted for beam peak combination. The rf input power was trimmed to the desired value and the coupler gap and magnet currents were also trimmed for peak beam output. Generally, one iteration was sufficient to obtain the peak performance conditions.

Results and Discussion

The parallel plate rf ion thruster is still in an exploratory stage and only preliminary results have been obtained. Because of the strong influence of magnetic field geometry upon dc thruster performance, [1], initial experiments have been in this direction. The coupling characteristics of the rf power to the plasma discharge leaves much room for improvement; however, this area remains to be explored.

Magnetic Field Distribution

Some general design rules regarding magnetic field distribution have been used for dc thrusters. The central region of the ionization chamber, particulary near the ion extraction grids, is preferably field-free to promote a uniform beam current density. A forward drift of the plasma ions to reduce losses is believed to be enhanced by a gradient in the magnetic field decreasing in the forward direction. In the radial direction, an increasing magnetic field tends to reflect electrons back into the ion chamber and leads to lower losses.

The magnet coils described in Apparatus and Procedures were used in an attempt to apply the above design rules. Effects of magnetic coil configuration and location are shown in Figure 2. The axial magnetic field strength on axis is plotted as a function of axial distance measured from the grid location. The distance between the two magnet coils was held fixed but their axial location was varied from 1.8 to 3.2 cm.

Initial attempts to produce a field with a steep gradient using two plain coils, (all-aluminum spool hereafter called "plain coil") of opposing polarity were unsuccessful, as indicated by the curves for configuration A. The numerals enclosed in parentheses denote the front and rear magnet currents, respectively, reading from left to right. A high reverse field in the rear coil tended to limit the peak field attainable. Reducing the rear coil current to obtain a high peak value also raised the field at the rear to undesirable levels. Attaching a soft-iron plate to the face of one of the coils to obtain a field-shunted coil (configuration B), hereafter referred to as a "shunted coil," permitted further shaping of the axial magnetic field. By adjusting the currents of the two

opposing field coils, it was possible to increase the peak to desired values and still cause a steep field gradient.

Movement of the coil assembly rearward (configuration C) shifted the position of the peak field accordingly. As the field currents indicate, a lower front coil current and higher rear coil current lowered the peak field and increased the rear gradient.

A two dimensional map of magnetic field contours within the right half plane along a thruster radius is shown in Figure 3 for the coil current (4.3;1.0). Each contour line is denoted with the absolute value of the magnetic field or the vector sum of the axial and transverse fields measured with Hall effect probes. Because the number of traverse points were limited, some degree of estimating has been employed. The general pattern evident is that the field was higher than desirable at the grid plane compared with favorable field distributions currently found in dc thrusters. The field increased in strength near the side wall as desired but, unfortunately, decreased in strength in the direction of the rear wall. The criticality of these field magnitudes and gradients is yet to be defined in both dc and ac thrusters.

Plain Coil Performance

Thruster performance obtained with the plain magnet coil (configuration A) is shown in Figure 4 as a function of the plasma gap between the coupler disk and the screen grid. The magnet coil currents were set to obtain the maximum beam current of 28 mA, seen in Figure 4(a). This maximum occurred at a gap of 2 cm. The discharge was either unstable at a gap less than 1.7 cm or could not be started at all. At gaps greater than 2 cm, the beam current dropped rapidly with a second lower peak at 2.8 cm.

The reflected power for constant incident power of 70 W is shown in Figure 4(b). No definite correlation could be drawn between reflected power and beam output level. More than 50 percent of the incident power was reflected back at all times, thus indicating a poor impedance match. Without the plasma discharge, however, practically 100 percent of the incident power was reflected.

As a matter of interest, the electron cyclotron frequency corresponding to the static axial magnetic field measured on-axis with no plasma present is shown in Figure 4(c). The input frequency of 150 MHz was less than the cyclotron frequency corresponding to the lowest axial magnetic field found in the thruster. Absolute values of magnetic field anywhere else in the thruster are expected to be higher, thus resulting in higher cyclotron frequencies.

Shunt Coil Performance

Thruster performance obtained by using the shunted magnetic field coil (configuration B and C) is shown in Figure 5. Beam current data for the two coil positions tested are presented in Figure 5(a). The front coil position indicated is the distance from the grid to the front coil centerline in centimeters. Clearly, the performance with the coils in the forward position (confifuration B) was superior. Similarly to the plain coil operating characteristics, (Figure 4), two peaks in the beam current output were observed. The higher peak occurred at a larger grid to coupler gap.

The reflected power for a constant incident power of 70 W, again, gave no clear evidence of trend or correlation as seen in Figure 5(b). In all instances, more than 50 percent of the incident power was reflected.

The magnetic field on-axis for the two magnet positions is shown in Figure 5(c). Electron cyclotron frequency for various levels of magnet field strength is also indicated. The two values of input frequency used are within the range of cyclotron frequencies corresponding to the static axial magnetic field measured in the thruster with no plasma. A strong argument cannot be made for the significance of these frequency numbers, particularly because in the plain coil configuration, described previously, the cyclotron frequency did not correspond to the input frequency. The beam current output was very sensitive to the gap between the grid and coupler plate, especially near the maximum value. Because wave length at the frequencies used is much larger than the gap, resonant lengths effects are excluded. It is of interest to examine the relationship between thruster performance and the static magnetic field, particulary in that region where the coupler plate position was found to be critical.

The effects of varying the magnet current in the front coil of configuration C, while holding a constant value of rear coil current and a fixed coupler position, are shown in Figure 6. The magnet coils were located in the rearward position for these tests. The beam current in Figure 6(a) also showed a highly peaked characteristic, dropping sharply on either side of the optimum value. The on-axis axial magnetic field at the coupler plate location is shown in Figure 6(c). The variation of the field was essentially linear with coil current as expected. The axial profile of the field undoubtedly changed slightly with varying coil current because of the presence of the opposing field from the rear coil. The electron cyclotron frequency corresponding to the on-axis axial magnetic field at the coupler did not match the input frequency of 142 MHz, but the sharply peaked behavior of the beam current as a function of magnetic field suggests a resonance effect occurring somewhere in the plasma generation region.

Similar results obtained while varying the rear coil current are shown in Figure 7. The beam current exhibited the same sharply peaked behavior. The axial magnetic field at the coupler plate, shown in Figure 7(c), decreased with increasing coil current because of its opposing polarity. The variation was essentially linear however.

The preceding discussion has shown sharply peaked performance effects, one of which had a geometrical dependence. For system considerations, variations in configuration or geometry are to be avoided in favor of electrical parameters which are more easily varied. It is of interest, therefore, to investigate the effects of input frequency and to determine what other parameters require adjustments to maintain peak performance.

Thruster performance with the two coil positions over a range of input frequency is shown in Figure 8. The incident power was kept at 70 W, and at each frequency, the coupler plate position and magnet coil currents were adjusted for peak beam output. Figure 8(a) shows that with the magnet coil in the forward, or 1.8-cm, position, the beam current increased with input frequency. With the coils in the rearward position, the output also increased with frequency initially, but reached a peak at about 142 MHz.

The reflected power shown in Figure 8(b) was essentially constant over the frequency range tested. A slight increase in reflected power was observed at the higher frequencies for the rearward magnet position. The coupler plate to gap distance required for the peak output at each input frequency is shown in Figure 8(c). For both magnet positions, the optimum gap was nearly insentive to input frequency.

The variations in the magnetic field coil currents to obtain peak output beam current at each frequency are shown in Figure 8(d). For both positions of the coils, the front coil current was essentially constant over the frequency range. The rear coil currents showed a decreasing trend as frequency increased. As seen in Figure 7(c), a decreasing rear coil current resulted in a higher on-axis magnetic field. Thus the electron-cyclotron frequency corresponding to this magnetic field would also increase in agreement with the increasing input frequency. Although not conclusive, available evidences point to the possible requirement of a resonance effect for peak performance operation.

The performance of configuration B at 150 MHz and different power levels is shown in Figure 9. For this test, the coupler plate position and magnet coil currents were held constant at the optimum values found at 70 W incident power. The beam current shown in Figure 9(a) increased monotonically but not linearly with incident power, rising less rapidly at higher power. At 100 W, the beam current was about 60 mA. The reflected power increased linearly with incident power as shown in Figure 9(b). An approximately constant 60 percent of the incident power was reflected over the operating range. Similarly, the fraction of incident power reflected during gap changes and input frequency variations was between 60 and 75 percent. The relatively constant fraction of incident power that was reflected over a wide range of plasma conditions tends to indicate that most of the reflected power was due to impedance mismatch in the coupling structure. The transition from the 50 ohm coaxial line to the coupler plate is a probable point of an abrupt and large impedance change.

The ion cost or discharge loss in watts per beam ampere is shown in Figure 9(c). The discharge loss based on absorbed power only was of the order of 525 to 625 W per beam ampere. Comparison data of an 8-cm-diam. dc discharge in argon are not known to be available. In 12- and 30-cm-diam. dc thrusters, the discharge losses are about 240 to 290 W/ per beam ampere. Whether or not the rf performance can be expected to improve with increasing thruster size is open to question. Other research areas need to be considered also.

One of the areas that need further work is impedance matching to reduce reflected power. Well established high frequency techniques such as tuning circuits and coaxial line transformers are available and could significantly improve performance.

Another area requiring investigation is sputter erosion. Of more concern than destructive sputtering is the coating of dielectric surfaces and consequent changes in impedance to the rf power. After several hours of operation, thruster performance was observed to change gradually. Cleaning the sputtered metal coating from the interior surface of the quartz liner restored original performance. Other investigators have used dielectric material to shield their antenna coil from the plasma.[6] A similar technique may be useful for the rf concept explored here. In the present design, the screen grid which was exposed to the plasma was both an electron collector and a source of sputtered material. A positive bias on the screen grid relative to a shadow-shielded electrode might serve to minimize ion sputtering of the screen grid. Another approach could use a dielectric-coated screen grid together with a shadow-shielded electron collector electrode.

As mentioned earlier, the magnetic field distribution in this thruster was far from optimum. Because of the E and H field structure resulting from the rf power, the best static magnetic field distribution may be considerably different from that of a dc thruster. Evidences of a strong effect of magnet field upon discharge performance indicate this to be one of the more promising areas of further research.

Concluding Remarks

A preliminary investigation was conducted on a high frequency argon plasma source utilizing parallel plates in a diode type configuration. Discharge losses of the existing preliminary 8-cm-diam. design are of the order of 525 to 625 W per beam ampere. Improvement of discharge performance is expected with additional research, especially by further changes in the static magnetic-field distribution.

Attractive features of the present approach are simplicity of construction plus use of small plasma dimensions and a variety of propellants. For applications where these features are overriding, the parallel plate ion thruster may be a viable candidate.

Areas of concern and question exist. Impedance-matching and power-coupling must be improved to reduce reflected power. The effects of sputtered-conductive film buildup need to be examined to assess performance changes and ultimately to eliminate the problem.

REFERENCES

1. Sovey, J. S., "Improved Ion Containment Using a Ring-Cusp Ion Thruster," AIAA Paper 82-1928, Nov. 1982.

2. Rawlin, V. K., "Operation of the J-Series Thruster Using Inert Gases" AIAA Paper 82-1929, Nov. 1982.

3. Steiner, G., "Development of a Large Inert Gas Ion Thruster," AIAA Paper 82-1927, Nov. 1982.

4. Loeb, H. W., "State of the Art and Recent Developments of the Radio Frequency Ion Motors," AIAA Paper 69-285, Mar. 1969.

5. Koschade, S. E., Pinks, W., Trojan, F., Loeb, H. W., and Bassner, H.W., "Development of a Flight Prototype of the R.F.-Ion Thruster RIT 10," AIAA Paper 72-471, Apr. 1972.

6. DiVergilio, W. F., Goede, H., Komatsu, G. K., and Christensen, T., "High Frequency Plasma Generators for Ion Thruster Applications, "AIAA Paper 81-0680, Apr. 1981.

7. Root, J., Rogers, J., Asmussen, J., and Hawley, M. C., "Fundamental Design Problems and Properties of Microwave Plasma/Ion Sources," AIAA Paper 81-0679, Apr. 1981.

8. Lee, R. Q., and Nakanishi, S., "Recent Work on an R.F. Ion Thruster," AIAA Paper 81-0678, Apr. 1981.

9. Byers, D. C., Kerslake, W. R., and Grobman, J.S., "Experimental Investigation of Heavy-molecule Propellants in an Electron-Bombardment thrustor," NASA TND-2401, (1964)

10. Kaufman, H. R., "Inert Gas Thrusters" Colorado State University, Fort Collins, CO)., July 1976. (NASA CR-135100).

11. Asmussen, J., Root, J., and Nakanishi, S.,"Performance Characteristics of a Microwave Plasma Disk Ion Source," AIAA Paper 82-1935, Nov. 1982.

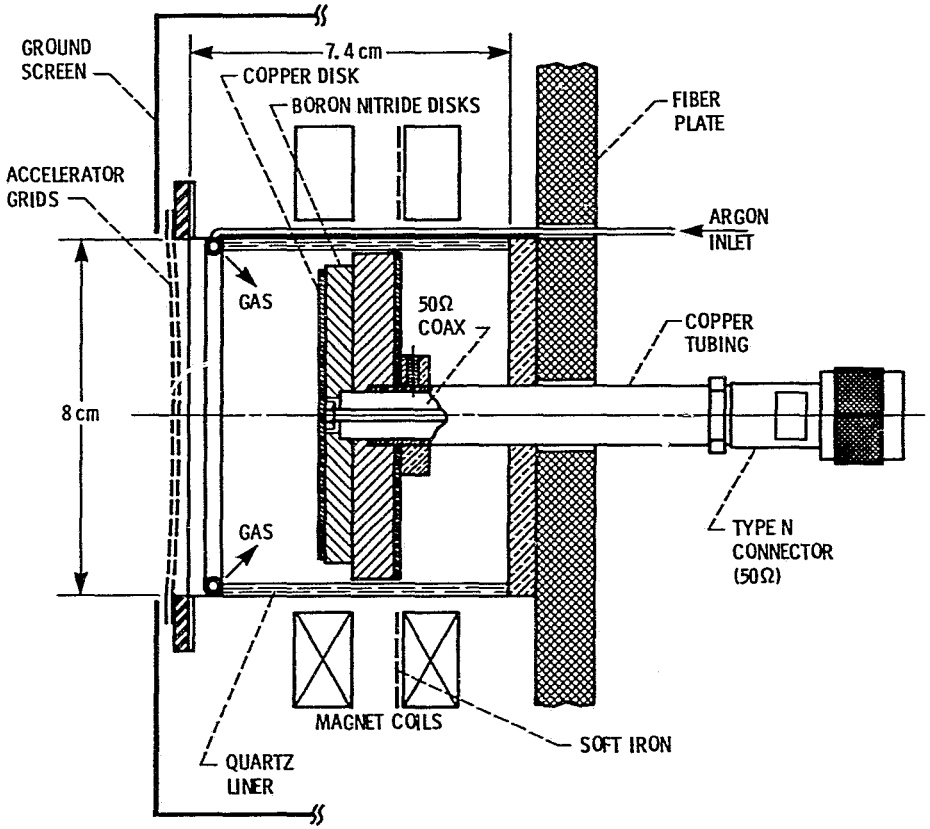

Figure 1. - Schematic cross-section of the parallel plate R.F. ion thruster.

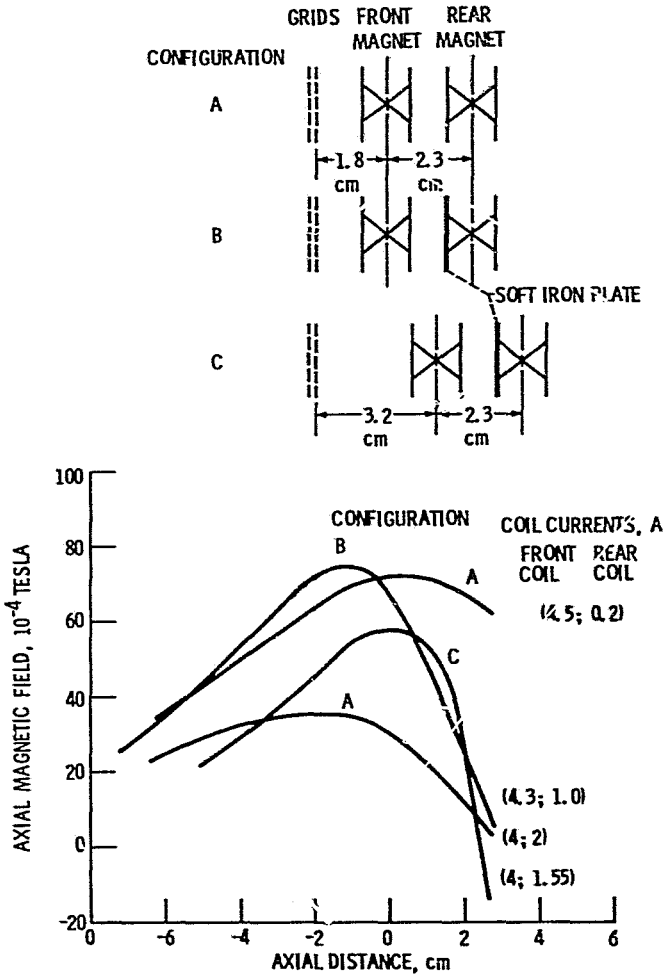

Figure 2. - Effects of magnet coil configuration and position on magnetic field distribution.

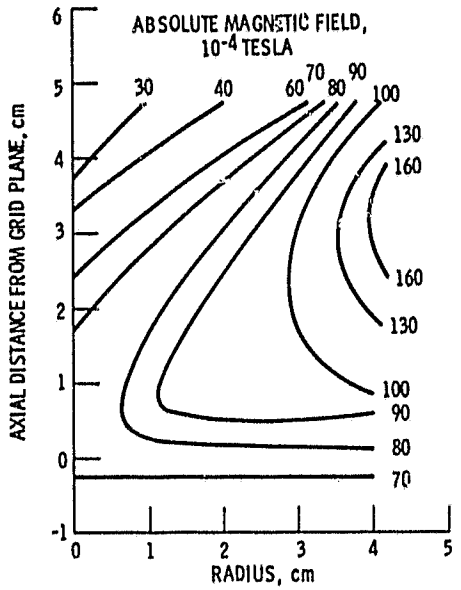

Figure 3. - Spatial distribution of absolute magnitude of static magnetic field within thruster. Front coil: 4.3 A; rear coil: 1.0 A.

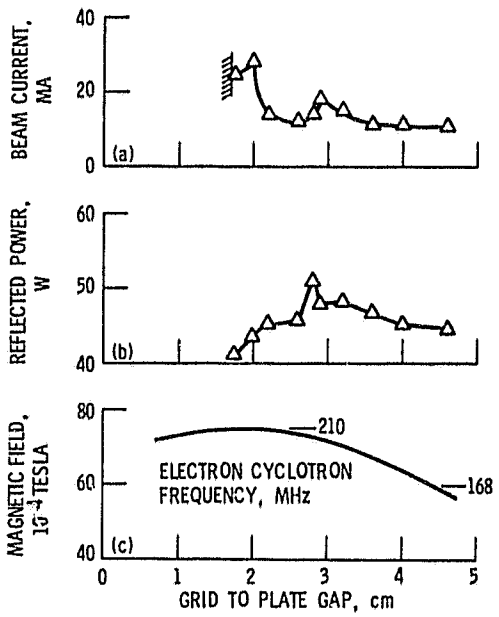

(a) Beam current.

(b) Reflected power.

(c) Axial magnetic field.

Figure 4. - Effect of gap with plain magnet coils (configuration A) adjusted for peak performance. Frequency, 150 MHz; incident power, 70W.

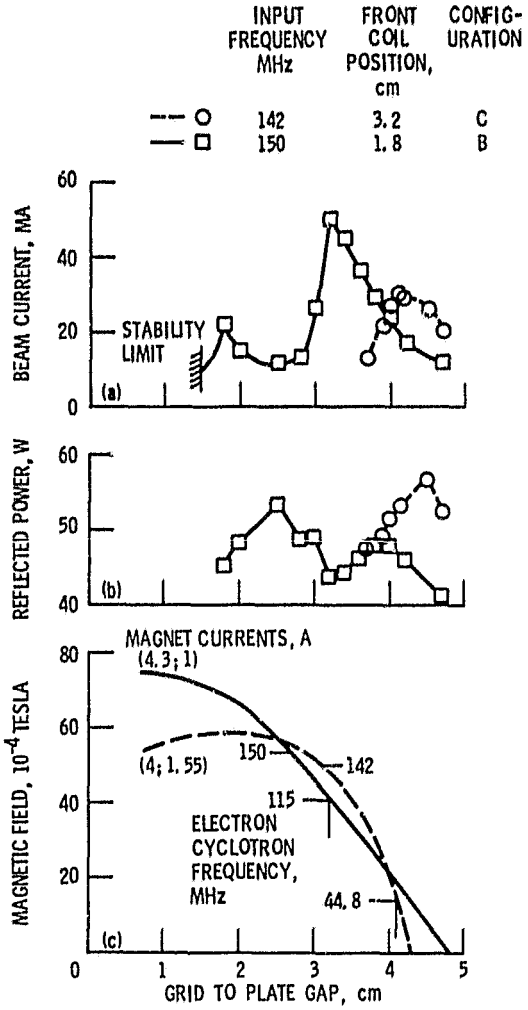

(a) Beam current.

(b) Reflected power.

(c) Axial magnetic field.

Figure 5. - Effects of gap with shunted magnet coil configurations B and C adjusted for peak performance. Incident power: 70W.

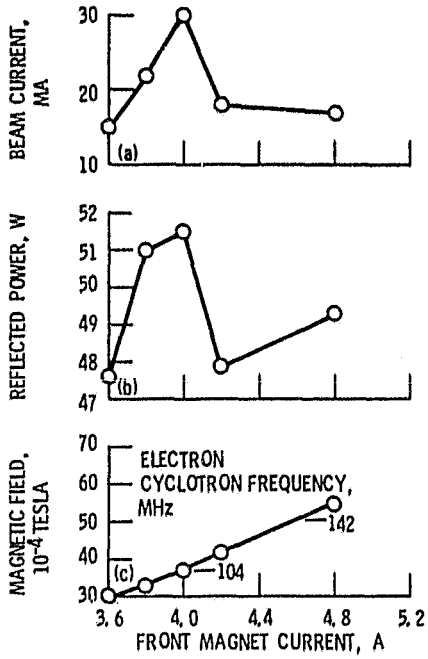

(a) Beam current.

(b) Reflected power.

(c) Axial magnetic field at coupler plate location.

Figure 6. - Effects of front magnet coil current in configuration C. Frequency, 142 MHz; incident power, 70W; rear coil current, 1.55 A.

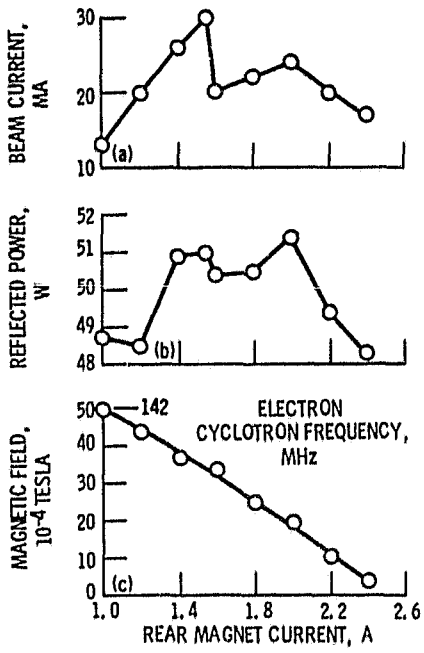

(a) Beam current.

(b) Reflected power.

(c) Axial magnetic field at coupler plate location.

Figure 7. - Effects of rear magnet coil current in configuration C. Frequency, 142 MHz; incident power, 70W; front coil current, 4.0 A.

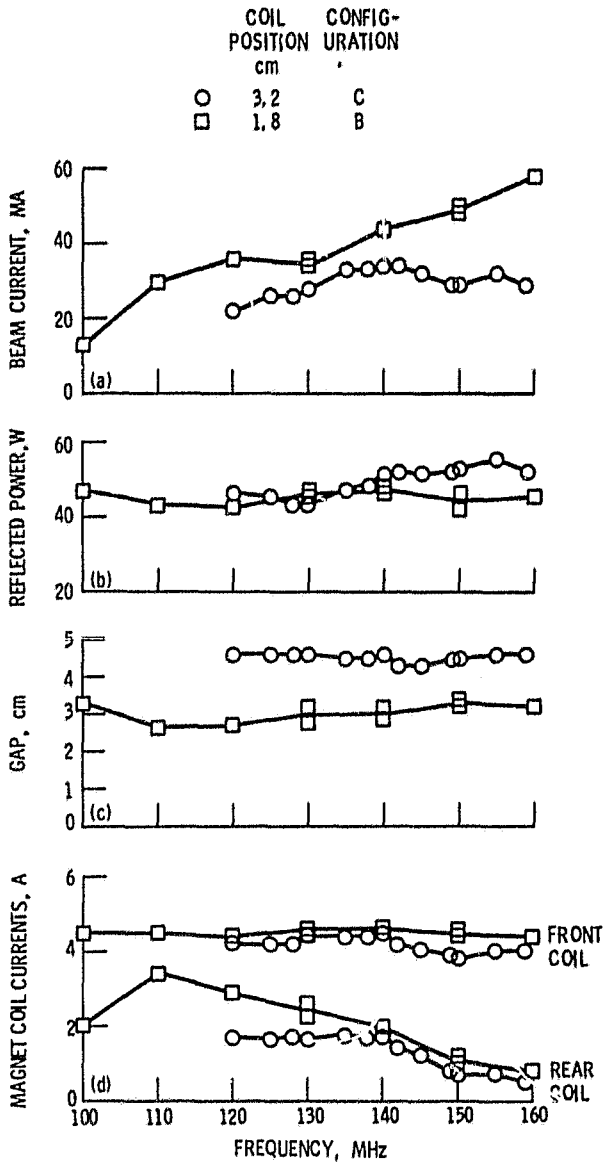

(a) Beam current.

(b) Reflected power.

(c) Grid to coupler gap.

(d) Magnet coil currents.

Figure 8. - Peak-beam operation at various input frequencies. Incident power, 70 W; argon flow, 1.37×10^{-7} kg/sec.

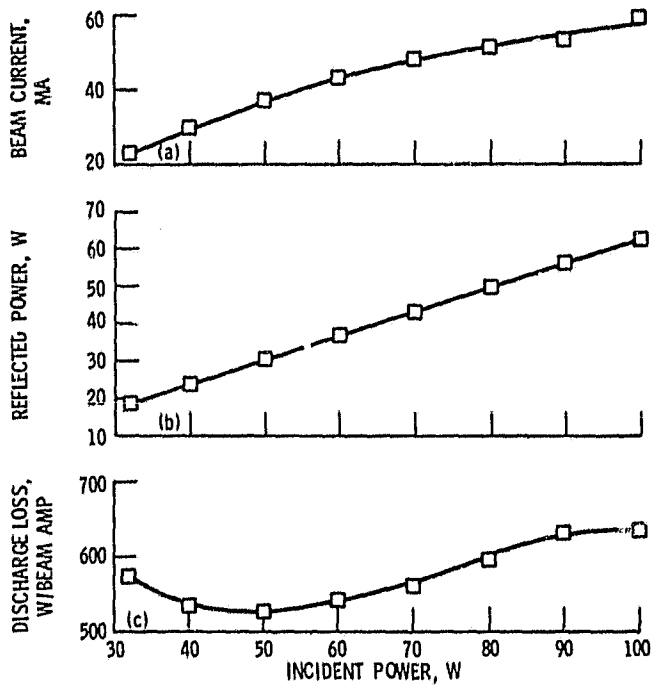

(a) Beam current.

(b) Reflected power.

(c) Discharge loss.

Figure 9. - Discharge performance of configuration B at various levels of incident power. Frequency, 150 MHz; grid to plate gap, 3.2 cm.